Sigma Journal of Engineering and Natural Sciences
Web page info: https://sigma.yildiz.edu.tr
DOI: 10.14744/sigma.2025.1912

Research Article

Effect of reinforcements in aluminium 5052-magnesium AZ31 explosive cladding

S. SARAVANAN[1]

[1]Department of Mechanical Engineering, Annamalai University, Annamalainagar, Tamilnadu, 608002, India

ARTICLE INFO

Article history
Received: 18 April 2024
Revised: 03 August 2024
Accepted: 13 October 2024

Keywords:
Aluminium 5052; Explosive Cladding; Magnesium AZ31; Microstructure. Silicon Carbide; Strength; Wire-Mesh

ABSTRACT

Aerospace, automobile, and marine industries prefer aluminium-magnesium weld joints for the fabrication of lightweight, corrosion-resistant structures. However, at elevated temperatures, they suffer from reduced strength and display potential for cracking. Hence, in this study, a innovative approach of combining explosive energy and reinforcement materials to improve the strength, thermal stability, ductility, and performance of the aluminium 5052-magnesium AZ31 clads, through explosive cladding is attempted. The interface micrograph of the conventional clad (no reinforcement) shows the continual presence of molten intermetallic layer. The layer formation is inhibited by introducing a stainless steel wire-mesh between the mating alloys, which reduces the velocity of the aluminium sheet owing to the enhanced friction. Similarly, the addition of silicon carbide particles along with the wire-mesh evades the straight impact of mating alloys and thereby suppresses the formation of reaction compounds. With respect to mechanical strength, the clad having both wire-mesh and silicon carbide reinforcement attains the maximum hardness (285 Hv), ram tensile (302 MPa), and shear strength (175 MPa), followed by wire-mesh-reinforced clad (hardness-245 Hv, tensile strength-254 MPa, shear strength-146 MPa), and conventional clad (hardness -98 Hv, tensile strength-102 MPa, shear strength-59 MPa).

Cite this article as: Saravanan S. Effect of reinforcements in aluminium 5052-magnesium AZ31 explosive cladding. Sigma J Eng Nat Sci 2025;43(6):2084–2093.

INTRODUCTION

Magnesium alloys are promising candidates in automobile, and aircraft manufacturing due to their lower density, higher strength, good machining ability, and high damping capacity [1]. In addition, magnesium alloys are eco-friendly in nature [2]. However, detrimental qualities, such as strong chemical vulnerability, low resistance to corrosion, poor room temperature ductility, and wear resistance, limit their industrial applications [3]. To counter this, magnesium is welded with other alloys, such as aluminium, in order to utilize the beneficial characteristics of both [4]. Aluminium alloys are preferred due to their better strength-to-weight ratio, greater resistance to corrosion, better plastic deformation capacity, and higher ductility [5]. The aluminium-magnesium weld joints are used to construct light weight corrosion resistant components in ship building, aircraft and automotive components. Earlier researchers

*Corresponding author.
*E-mail address: ssvcdm@gmail.com

This paper was recommended for publication in revised form by Editor-in-Chief Ahmet Selim Dalkilic

employed various welding techniques to join aluminium and magnesium and are recapitulated below.

In an earlier study, Wang et al. attempted Al-Mg laser welding and reported the presence of γ-$Mg_{17}Al_{12}$ and β-Mg_2Al_3 compounds, which affected the strength adversely [6]. To mitigate the intermetallic compound formation, Meng et al. successfully employed a titanium interlayer between Al and Mg alloys in the laser-arc hybrid lap welding [7]. Likewise, a similar result was obtained by Kumar and Wu, who performed friction stir welding with a nickel interlayer [8]. Varmazyar and Khodaei, on the other hand, used a copper interlayer in diffusion bonding of Al-Mg alloys at various strain conditions (0, 30, and 60%) and holding durations. They concluded that the interlayer reduces the hardness and shear strength [9]. In order to attain higher strength and a defect-free Al 1050–AZ31 alloy magnetic pulse weld, Zhu et al. optimized the process parameters, such as discharge energy and standoff distance [10]. In this context, Jian et al. analyzed the fatigue crack behavior in Al-Mg metal inert-gas welding. They concluded that the stress, bubble formation, orientation of the grain, and coarse grain formation dictated the crack growth [11]. Meanwhile, Liang et al., while friction welding Al-Mg alloys, determined the correlation between constitutional liquation and microstructure [12]. Based on the literature, the main challenge in Al-Mg welding is the development of deleterious reaction compounds and crack formation, which impacts the weld strength negatively. To counter this, explosive cladding provides a feasible solution due to its rapidity and ability to clad larger areas.

With respect to Al-Mg explosive cladding, the metallurgical, mechanical, and corrosion properties of AZ31-Al 5005 clad were studied by Acarer et al. [13]. Meanwhile, Chen et al. concluded that the process parameters, such as explosive mass and standoff distance, are directly proportional to the clad strength [14]. Similarly, Ghaderi et al. [15] developed a welding window and correlated the microstructure and strength characteristics with its positioning [16]. In this context, Paul et al. attempted explosive cladding of eleven Al-Mg foil layers and reported cracks and poor formability due to inadequate energy [17]. In a different attempt, Zeng et al. conducted their explosive cladding trials in a helium atmosphere and obtained superior mechanical properties [15]. Numerical simulation of Al-Mg explosive cladding was separately attempted by Feng et al. [18] and Kumar et al. [1] to determine the temperature and pressure created during the process. In a recent study, Su et al. observed delamination due to impact in Al-Mg explosive cladding [19]. The novelty of this study lies in the innovative use of wire-mesh and silicon carbide reinforcements in the explosive cladding of aluminium-magnesium alloys. By integrating these reinforcements, the study aims to enhance the microstructural refinement and mechanical properties of the clad. The combination of explosive energy and reinforced materials creates a unique interfacial bonding mechanism that improves strength, hardness, and corrosion resistance. This approach offers a new pathway for producing high-performance clad materials with tailored properties, suitable for applications in industries like aerospace, automotive, and defence where lightweight yet strong materials are crucial.

MATERIALS AND METHODS

Al 5052 sheets (chemical composition wt. %: Si-0.25, Mg-2.9, Cr-0.25, Cu-0.1, Mn-0.1, Zn-0.1, Fe-0.4, Al-Bal.) and AZ 31B plates (chemical composition wt. %: Al-2.8, Zn-1.75, Si-0.1, Mn-0.2, Cu-0.05, Mg-Bal.), purchased from Parshwamani Metals, Mumbai, India, were employed as flyer and base plate, respectively. The dimensions of the flyer and base plate are 110 mm x 80 mm (length x breadth), with thicknesses of 2 mm and 6 mm, respectively.

Three explosive cladding experiments, viz., Al-Mg, Al-Mg with stainless steel wire-mesh (purchased from Sysco Piping Solutions Inc., Mumbai, India), and Al-Mg with stainless steel wire-mesh (mesh size of 0.704 mm) and SiC (purchased from Parshwamani Metals, Mumbai, India: 100-120 μm size), were performed at a uniform loading ratio, R (ratio of the mass of the explosive and flyer plate) of 0.8 and 5 mm standoff distance, SD (between flyer and base plates). The parameters were chosen based on preliminary experimental trials. The energy source was the SUN 90 chemical explosive (manufactured by M/s. Vetrivel Explosives Private Limited) having a density of 1.15 g/cm^3 and a detonation velocity of 4200 m/s and was mounted on a 2 mm thick cardboard buffer plate. The reinforcements, viz., stainless steel wire-mesh (chemical composition wt. %: C-0.085, Cr-18, Mn-2, Mo-3, Ni-14, Si-1, S-0.03, Fe-Bal.) of dimension (110 x 80 mm x 0.3 mm) and SiC (micrograph shown in Fig.1) having 1% by weight of flyer plate, are dispersed, separately and together, on the base plate and were cladded by parallel explosive cladding (Fig. 1). Further increase in SiC reinforcements resulted in agglomeration resulting in increased brittleness.

Prior to cladding, the participant alloys and stainless steel wire-mesh (Fig. 2a) were annealed for one hour, followed by furnace cooling (Wire-mesh-900^{0}C, Al-400^{0}C, AZ31B-425^{0}C) to homogenize the metallurgical structure. To ensure good quality, the roughness of the mating surfaces is maintained below 1 μm. Based on the experimental parameters of the welding window, an analytical estimation to determine the nature of the explosive clad interface is determined. The welding window comprises lower and upper boundaries, which are calculated by equations 1 and 2, respectively [20, 21].

$$\beta = 1.14\sqrt{\frac{H_V}{\rho V_C^2}} \quad (1)$$

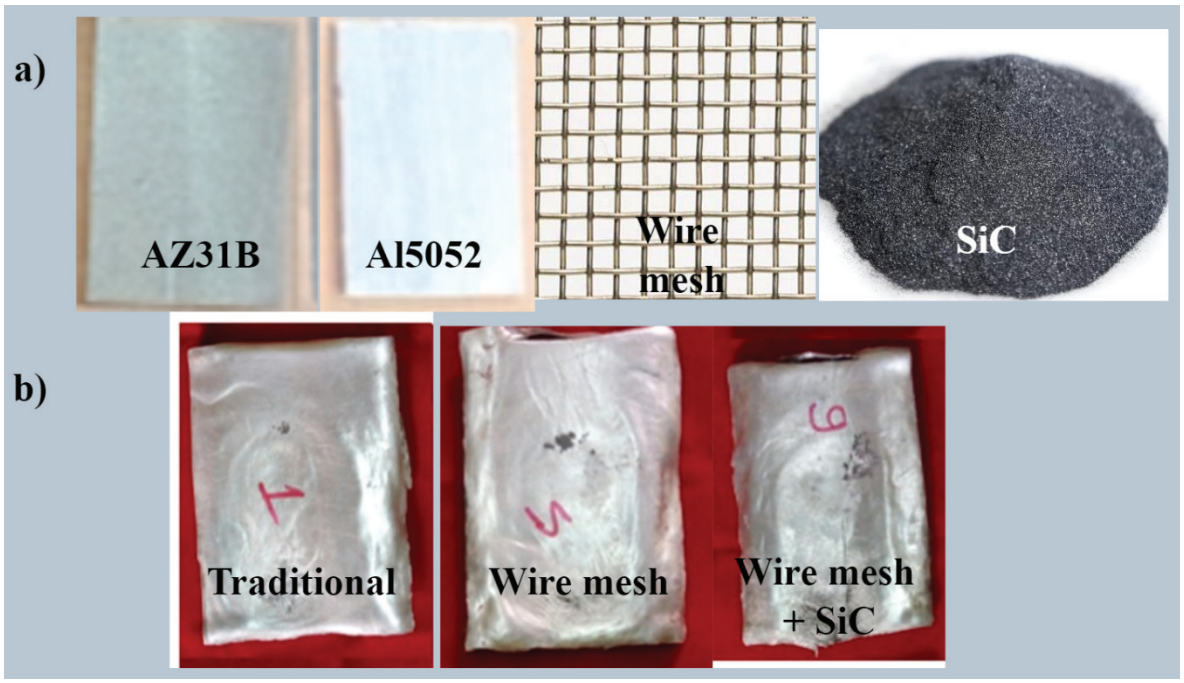

Figure 2. (a) Participant alloys and inclusions (b) explosive clads.

$$\sin\frac{\beta}{2} = \frac{k_3}{\left(t^{0.25}.V_C^{\ 1.25}\right)} \quad (2)$$

Where k_3 =C_f/2, $C_f = \sqrt{K/\rho}$, K= E/3(1-2ν),

The flyer plate moves towards the base plate obliquely at angle β, which is calculated by [22]

$$\beta = 2\sin^{-1}\frac{V_p}{2V_d} \quad (3)$$

Where the flyer plate velocity, V_p is determined by [23]

$$V_p = V_d\,\frac{0.612R}{(2+R)} \quad (4)$$

The experimental conditions attempted in the study are shown as green triangle, which falls inside the boundaries of the welding window (Fig. 3). The photographs of the resulting explosive clads are shown in Figure 2b.

After cladding, the specimens were subjected to standard metallographic procedures and etched for 30 seconds. A VERSAMET optical microscope and a JOEL

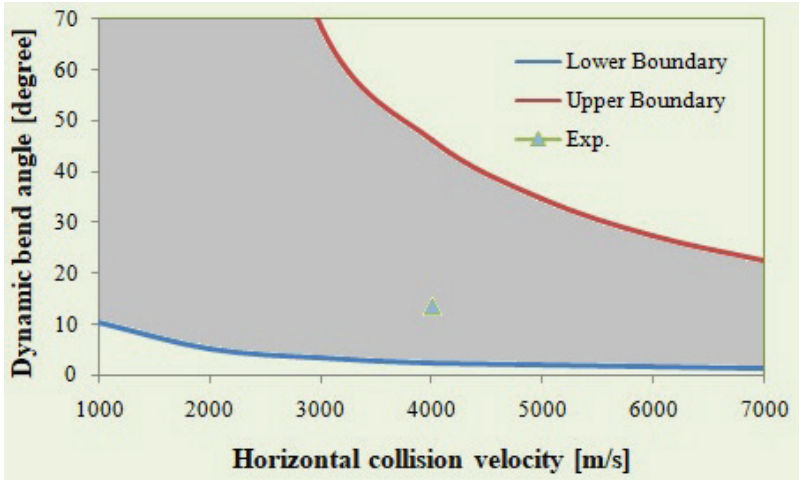

Figure 3. Welding window for Al 5052-AZ 31B explosive cladding.

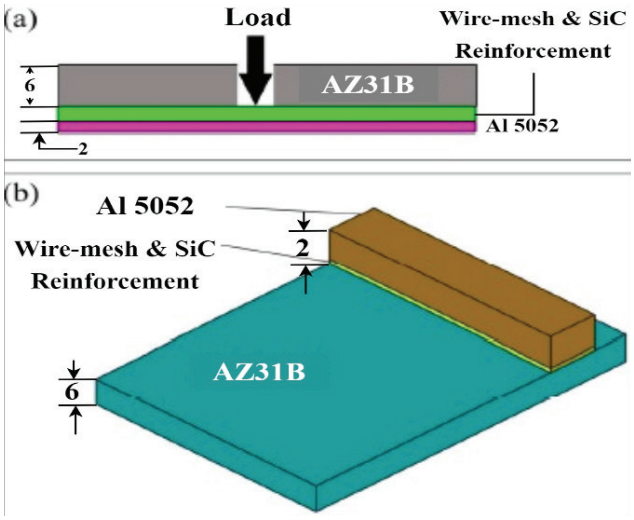

Figure 4. (a) Ram tensile test (b) Shear test.

(JSM-6610LV) scanning electron microscope equipped with EDS were utilized to analyze the microstructures. The constituents of various phases in the interface were identified with a CuK-equipped XRD (Philips X'PERT MPD diffractometer). The phases present in the sample are identified by comparing the observed diffraction peaks with standard reference card numbers. A ZWICK micro-hardness tester with an indenter load of 50g for 10s determines the Vickers hardness across the interface. Ram tensile (Fig. 4 a: MIL-J-24445A) and shear (Fig. 4b: ASTM B 898) tests were performed using 0.2 mm/min and 0.5 mm/min tensile and shear loads, respectively.

RESULTS AND DISCUSSION

Micrograph of the Conventional Al 5052-AZ31B Explosive Clad

The dissimilar explosive clad interface micrograph reveals an undulating nature along with an incessant molten layer (Fig. 5a). The molten layer, weak and fragile regions, is formed due to the utilization of whole kinetic energy (ΔKE) at the interface (0.79 MJ/m^2) followed by rapid cooling. The kinetic energy utilization is analytically determined by [24],

$$\Delta KE = \frac{m_f m_b V_p^2}{2(m_f + m_b)} \quad (5)$$

The effective utilization of kinetic energy promotes a wavy interface; otherwise, a molten layer is formed, as seen in Fig. 5a, if the additional kinetic energy is utilized. Somasundaram et al., while cladding titanium-steel, also observed a streak of molten layer at a higher kinetic energy environment, consistent with the present study [25]. The presence of a molten layer holds a negative impact on the strength characteristics, detailed in sections 3.3 and 3.4.

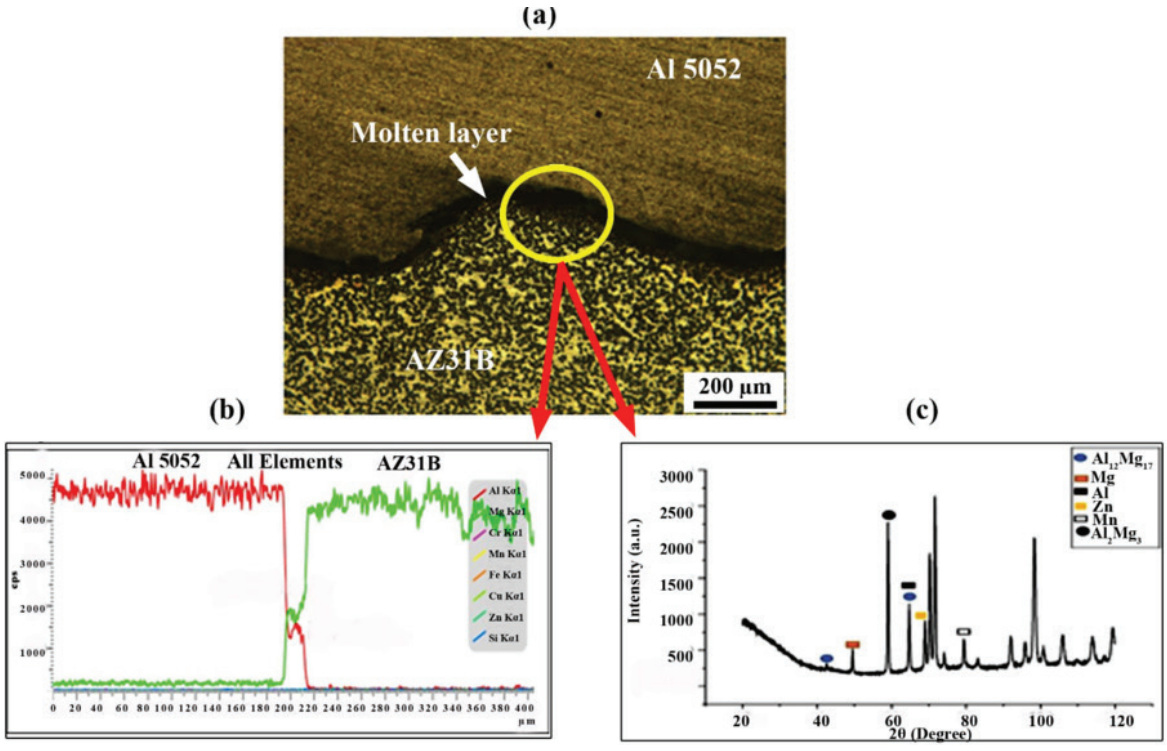

Figure 5. (a) Al 5052-AZ 31B micrograph (b) EDS (c) XRD.

The interface region (depicted by a circle in Fig. 5b) subjected to the EDS examination confirmed higher atomic percentages of aluminium and magnesium, along with a very lower concentration of Cr, Mn, Fe, Cu, and Si elements. Further analysis by the XRD (Fig. 5c) substantiates the existence of $Al_{12}Mg_{17}$ and Al_2Mg_3 compounds (card number: 00-025-1207) at the interface. To counter the intermetallic compound formation, reinforcements are introduced between the mating alloys, and the results are presented below.

Effect of Reinforcements on the Interface Micrograph

The variation in dissimilar clad micrographs, with and without reinforcements for the same parametric conditions, is noteworthy and obvious. The continuous presence of molten layer found in Al 5052-AZ 31B cladding (Fig. 5) is absent in the clads having reinforcements (Fig. 6, 7). The SiC is visible as a black strip, while the stainless steel wire-mesh is seen as white oval dots.

The insertion of a stainless steel wire-mesh transforms the molten layer prevailed in Al 5052-AZ 31B explosive clad into a defect free clad (Fig. 6 a,b). The dynamic collision of aluminium sheet with the wire-mesh instead of magnesium plate, promotes this transformation. The surface variations on the wire-mesh enhance the friction, and reduce the flyer plate velocity (V_p). In addition, the weight of the base plate, m_b (Eq. 5) increases as well. As a consequence, ΔKE improves to 0.81 MJ/m^2, and hinders the interfacial molten layer. The XRD (Fig. 6 c) analysis displays taller Fe, Mg, and Al peaks and a smaller Fe_3Al peak (card number: 03-065-1477). The marginal presence of reaction compounds at the interface is consistent with Gulenc et al [26].

The usage of both stainless steel wire-mesh and SiC particles, as reinforcements, on the base plate further increases the weight of the base plate (m_b), and hence ΔKE (Eq. 5) increases to 0.83 MJ/m^2. The increased ΔKE deforms the SiC particles further, forcing them to trap inside the openings in stainless steel wire-mesh, visible as a thin black strip (Figs. 7 a and b). This band formation at the interface by the SiC particles is consistent with earlier researchers [27, 28].

In addition, the primary chemical relationship between wire-mesh and SiC is quite weak [29]. Subsequently, an intermetallic free clad emerges between the flyer and base plates. The superior thermal conductivity, K of SiC (350 W/mK), accelerates the solidification and prevents the formation of a molten layer as well. The XRD spectrum confirms the existence of Fe, Al, and SiC elements at the interface and the nonexistence of element diffusion across the alloys (Fig. 7c). Since the SiC streak prevents the direct contact, the intermetallic compounds formed in the Al-Mg clad without reinforcements are eliminated. Further, the higher

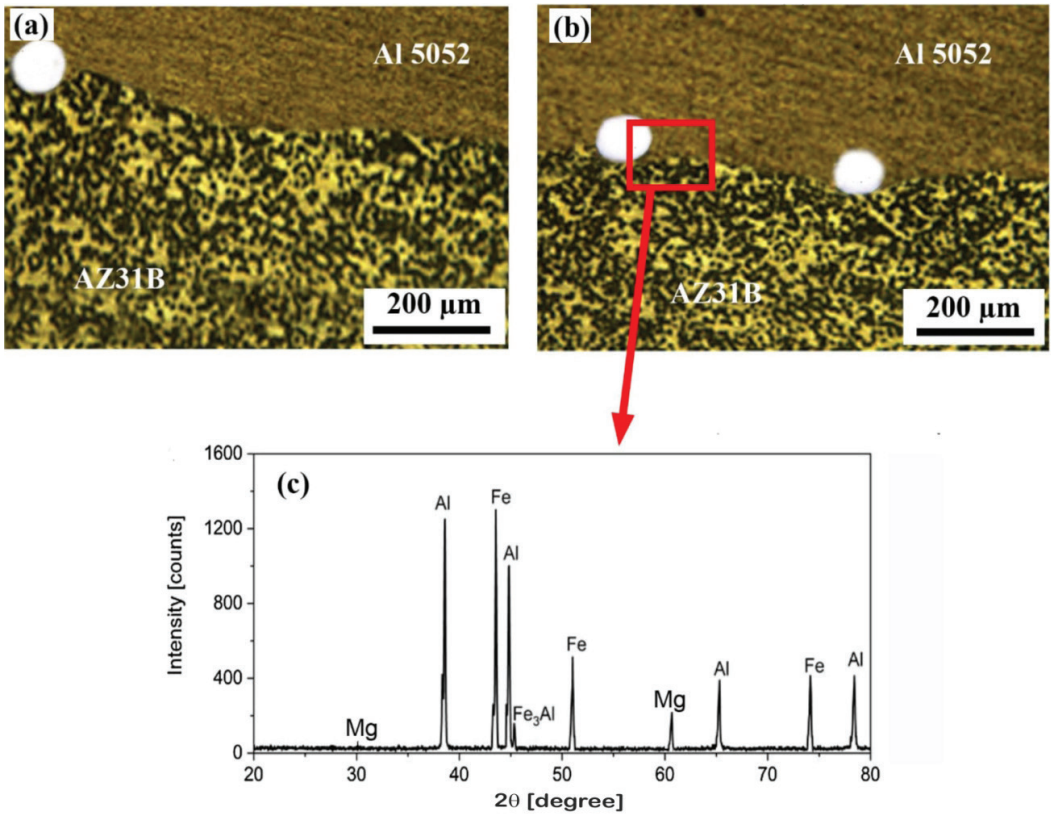

Figure 6. (a,b) Al 5052-WM-AZ 31B explosive clad micrograph (c) XRD.

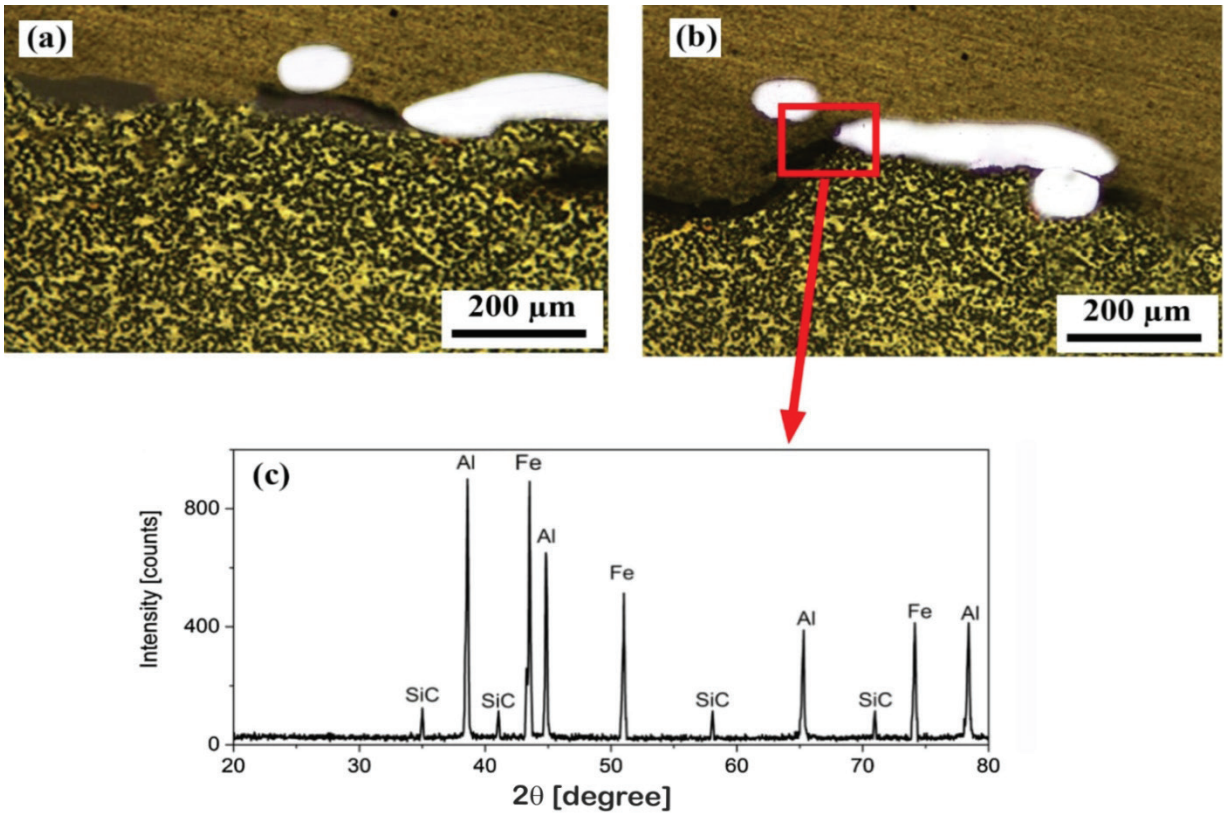

Figure 7. (a,b) Al 5052--AZ 31B explosive clad microstructure with wire-mesh and SiC reinforcements (c) XRD.

strength of these reinforcements improves the strength of the dissimilar clads, detailed in the next section.

Hardness

The average of two hardness measurements across the dissimilar reinforced explosive clad is higher than the clad having no reinforcements (Fig. 8). Further, the highest hardness is observed at the interfaces in all three experiments. The augment is attributed to the sudden impact and the existence of reinforcements. In addition, the rapid nature of the process restricts the interface to experiencing the increase in temperature. As a result, the impact of annealing is mitigated, and hence the hardness of the interface increases.

The interface of the stainless steel wire-mesh and SiC reinforced clad (Fig. 8c: 285 H_v) achieves the highest hardness as both reinforcements have great adhesion to the participating alloys. The existence of wire-mesh and the absence of SiC reduce the interface hardness by 16% to result in a hardness of 245 H_v (Fig. 8 b). The hardness of the Al 5052-WM-AZ 31B interfaces devoid of wire-mesh attains 120H_v, which is higher than the Al-Mg explosive clads (Fig. 8 a: 98Hv). However, the lower interface hardness is higher than the base alloys (Al -68 H_v and Mg -76 H_v), consistent with Inao et al [30]. Further, it is noted that the increase is not evident at locations 200 µm distant from the interface owing to the negligible plastic deformation, as reported by Chen et al. [31].

Ram Tensile and Shear Strengths

Figure 9 illustrate the ram tensile and shear strengths of the parent alloys and the dissimilar explosive clads attempted (stress-strain curves are given in Fig. 10). The use of reinforcements enhanced the ram tensile and shear strengths of the clads, and the maximum is obtained when both wire-mesh and SiC are reinforced (ram tensile-302 MPa, shear strengths-175 MPa). This is due to the cohesiveness of reinforcements and the absence of intermetallic compounds.

The Al 5052-AZ 31B explosive clad reinforced with a wire-mesh attains an 18% lower strength (ram tensile-254 MPa and shear-146 MPa). The reduction in strength is due to the absence of SiC particles. However, the obtained values are higher than the conventional Al 5052-AZ 31B explosive clad (102 MPa and 59 MPa) and base alloys. The reports of earlier researchers who attempted dissimilar cladding are consistent with this behaviour [32, 33].

The fractograph of Al 5052-AZ 31B explosive clad obtained from the ram tensile test (Fig. 11a) reveals a ductile fracture mode with a cup-cone shape. The fracture surface is dominated by a uniform distribution of bigger aluminium (flyer plate) shatter, confirming its larger flow before

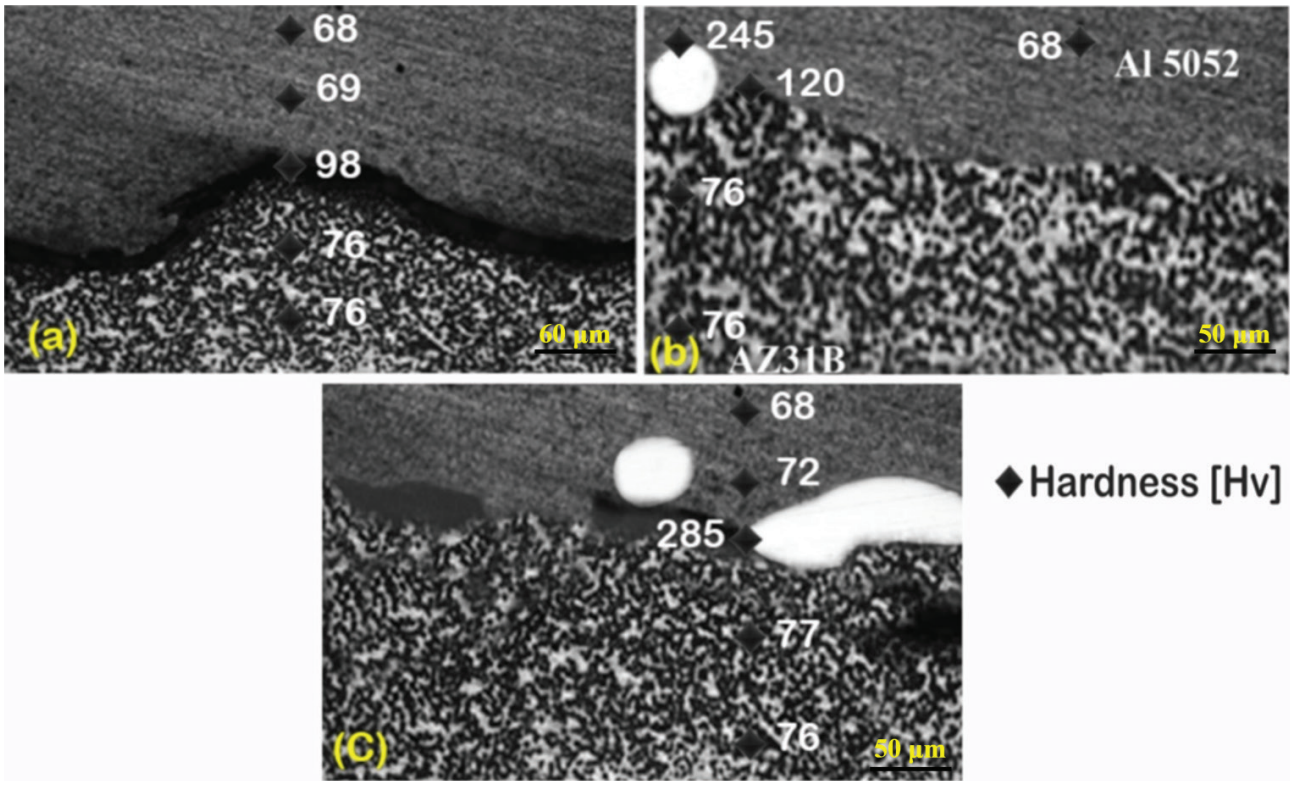

Figure 8. Hardness variation across the interface (a) Al 5052-AZ 31B (b) Al 5052-SS WM-AZ 31B (c) Al 5052-SS WM-SiC-AZ 31B .

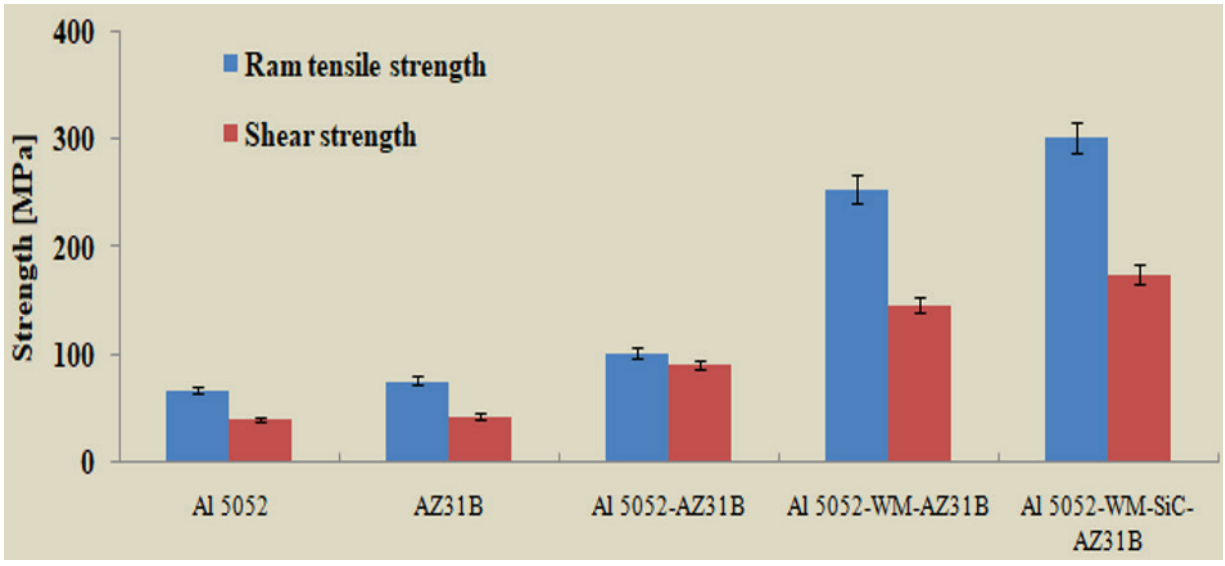

Figure 9. Ram tensile and shear strengths of the base alloys and explosive clads.

fracture. The impression created by the pulling of wires is visible in the fracture surface of the wire-mesh reinforced clad (Fig. 11b). Also, the fracture surface exhibits the evidence for a ductile mode of fracture. No significant defects are seen on the fractured surface. The fracture image of the Al 5052-WM-SiC-AZ31B explosive clad (Fig. 11c) is free from cleavage or intergranular fracture characteristics of the brittle fracture, as stated by Kumar et al [34]. Likewise, the evidence of wire-mesh and SiC sheared surfaces (Fig. 11d) with fibrous networks along with dimples is seen on

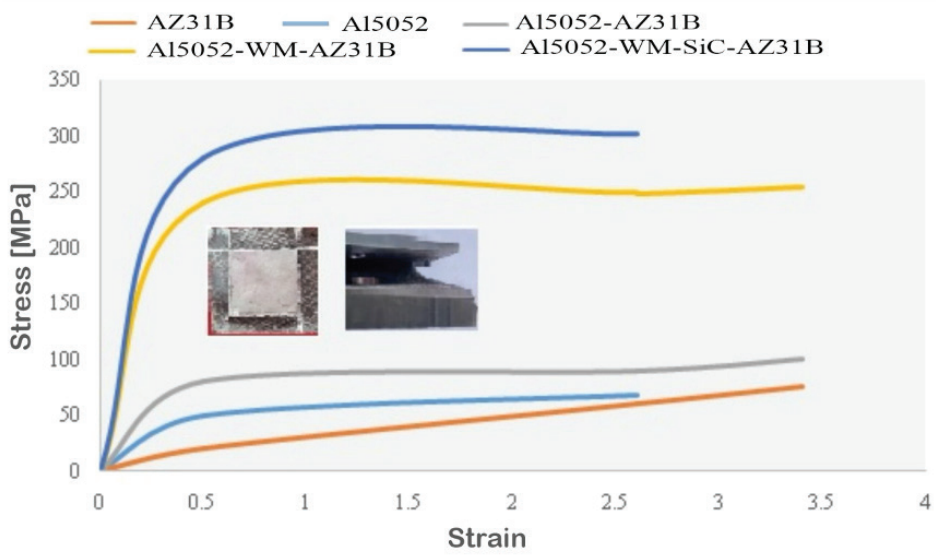

Figure 10. Stress-strain curve.

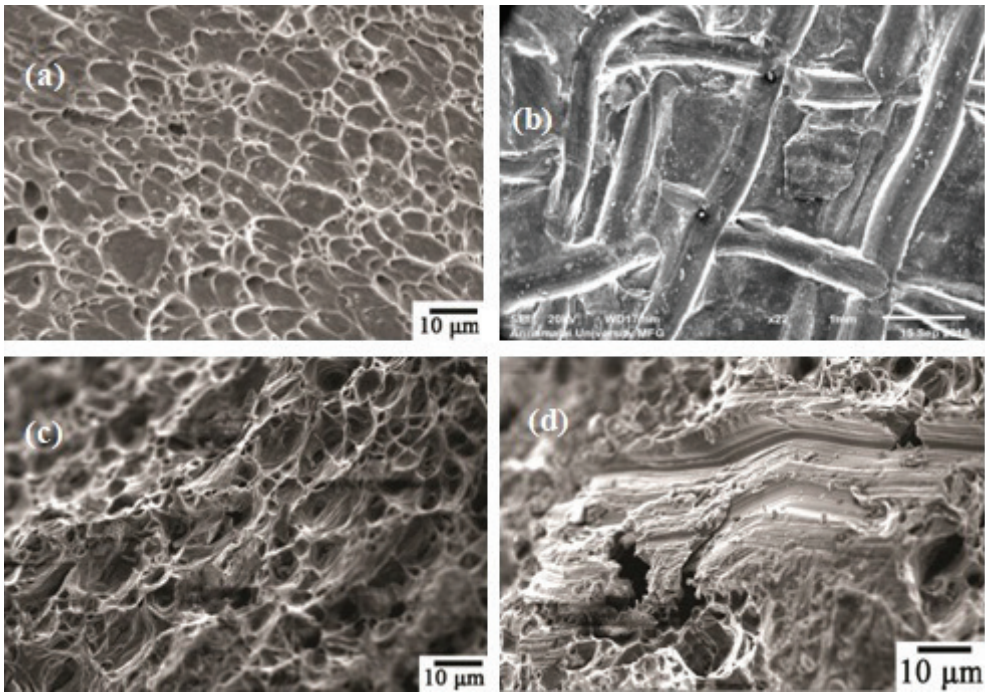

Figure 11. (a-c) Ram tensile interface fracture (a) Al 5052-AZ31B (b) with wire-mesh (c) with wire-mesh and Sic (d) Shear fracture surface of wire-mesh and SiC.

the shear surface obtained from the dissimilar explosive clad.

Therefore, we conclude that the industry offers significant potential for the application of SiC and wire-mesh reinforced Al/Mg explosive clad due to its ability to create strong, lightweight, and corrosion-resistant materials. The scalability of explosive cladding hinges on optimizing the process parameters to attain larger plates, enabling mass production. The long-term benefits such as reduced material waste, improved performance, and durability make it attractive. Explosive cladding of Al/Mg is suitable for aerospace, automotive, and marine industries where light weight coupled with high-performance materials are inevitable.

CONCLUSION

The salient findings of the novel study on the usage of reinforcements in explosive cladding of aluminium 5052-magnesium AZ31B explosive cladding are summarized here. The use of reinforcements in explosive cladding of weaker aluminium and magnesium alloys reduce the intermetallic formation and improve the ram tensile and shear strengths. The friction between the aluminium and magnesium is improved by the insertion of wire-mesh due to its potholed nature. Subsequently, the wire-mesh penetrates inside the mating alloys to create a strong bond. The silicon carbide particles form a band between dissimilar alloys to avoid the formation of reaction compounds, resulting in improved ram tensile (302 MPa) and shear (175 MPa) strengths. It is recommended to employ reinforcements in aluminium-magnesium explosive cladding.

NOMENCLATURE

ΔKE	Kinetic energy available (MJ/m^2)
Al	Aluminium
C	Carbon
$C_2H_2O_4$	Oxalic acid
C_f	Compressive wave velocity (m/s)
CH_3COOH	Acetic acid
Cr	Chromium
Cu	Copper
E	Young's modulus (N/m^2)
EDS	Energy Dispersive Spectroscope
Fe	Iron
H_v	Vickers hardness (N/m^2)
m_b	Mass of the base plate per unit area
m_f	Mass of the flyer plate per unit area
Mg	Magnesium
Mn	Manganese
Mo	Molybdenum
NaOH	Sodium hydroxide
Ni	Nickel
R	Loading ratio (mass of explosive /mass of flyer plate)
S	Sulfur
SD	Standoff distance (mm)
SEM	Scanning Electron Microscope
Si	Silicon
SiC	Silicon carbide particle
t	Flyer plate thickness
V_c	Collision point velocity(m/s)
V_d	Detonation velocity of the explosive
V_p	Velocity of the flyer plate (m/s)
WM	Wire-mesh
XRD	X-ray diffraction
Zn	Zinc
β	Dynamic bend angle (degree)
v	Poisson's ratio
ρ	Density (kg/m^3)

AUTHORSHIP CONTRIBUTIONS

Authors equally contributed to this work.

DATA AVAILABILITY STATEMENT

The authors confirm that the data that supports the findings of this study are available within the article. Raw data that support the finding of this study are available from the corresponding author, upon reasonable request.

CONFLICT OF INTEREST

The author declared no potential conflicts of interest with respect to the research, authorship, and/or publication of this article.

ETHICS

There are no ethical issues with the publication of this manuscript.

STATEMENT ON THE USE OF ARTIFICIAL INTELLIGENCE

Artificial intelligence was not used in the preparation of the article.

REFERENCES

[1] Kumar P, Ghosh SK, Saravanan S, Barma JD. Experimental and simulation studies on explosive welding of AZ31B-Al 5052 alloys. Int J Adv Manuf Technol 2023;127:2387–2399. [CrossRef]

[2] Jin Q, Tian G, Li J, Zhao Y, Yan H. The study on corrosion resistance of superhydrophobic magnesium hydroxide coating on AZ31B magnesium alloy. Colloids Surf A Physicochem Eng Asp 2019;577:8–16. [CrossRef]

[3] Sairam YNV, Cherukuri TS, Kurra HP. A short review on magnesium alloys in multiple domains. Sigma J Eng Nat Sci 2023;41:1062–1069.

[4] Liu L, Ren D, Liu F. A review of dissimilar welding techniques for magnesium alloys to aluminum alloys. Materials 2014;7:3735–3757. [CrossRef]

[5] Saravanan S, Gajalakshmi K. Soft computing approaches for comparative prediction of ram tensile and shear strength in aluminium–stainless steel explosive cladding. Arch Civil Mech Eng 2022;22:1–16. [CrossRef]

[6] Wang HY, Liu LM, Jia ZY. The influence of adhesive on the Al alloy in laser weld bonding Mg–Al process. J Mater Sci 2011;46:5534–5540. [CrossRef]

[7] Meng Y, Lu Y, Li Z, Zhao S, Gao M. Effects of beam oscillation on interface layer and mechanical properties of laser-arc hybrid lap welded Al/Mg dissimilar metals. Intermetallics 2021;133:107175. [CrossRef]

[8] Kumar S, Wu C. Eliminating intermetallic compounds via Ni interlayer during friction stir welding of dissimilar Mg/Al alloys. J Mater Res Technol 2021;15:4353–4369. [CrossRef]
[9] Varmazyar J, Khodaei M. Diffusion bonding of aluminum–magnesium using cold rolled copper interlayer. J Alloys Compd 2019;773:838–843. [CrossRef]
[10] Zhu C, Xu S, Gao W, Meng Y, Lin S, Dai L. Microstructure characteristics and mechanical properties of Al/Mg joints manufactured by magnetic pulse welding. J Magnes Alloy 2023;11:2366–2375. [CrossRef]
[11] Jian H, Wang Y, Yang X, Xiao K. Microstructure and fatigue crack growth behavior in welding joint of Al–Mg alloy. Eng Fail Anal 2021;120:105034. [CrossRef]
[12] Liang Z, Qin G, Ma H, Yang F, Ao Z. The constitutional liquation at the interface of Al/Mg friction welding joints. Sci Technol Weld Join 2017;22:363–372. [CrossRef]
[13] Acarer M, Demir B, Dikici B, Salur E. Microstructure, mechanical properties, and corrosion resistance of an explosively welded Mg–Al composite. J Magnes Alloy 2022;10:1086–1095. [CrossRef]
[14] Chen P, Feng J, Zhou Q, An E, Li J, Yuan Y, Ou S. Investigation on the explosive welding of 1100 aluminum alloy and AZ31 magnesium alloy. J Mater Eng Perform 2016;25:2635–2641. [CrossRef]
[15] Ghaderi SH, Mori A, Hokamoto K. Analysis of explosively welded aluminum–AZ31 magnesium alloy joints. Mater Trans 2008;49:1142–1147. [CrossRef]
[16] Paul H, Petrzak P, Chulist R, Maj Ł, Mania I, Prażmowski M. Effect of impact loading and heat treatment on microstructure and properties of multi-layered AZ31/AA1050 plates fabricated by single-shot explosive welding. Mater Des 2022;214:110411. [CrossRef]
[17] Zeng XY, Wang YX, Li XQ, Li XJ, Zhao TJ. Effect of inert gas-shielding on the interface and mechanical properties of Mg/Al explosive welding composite plate. J Manuf Process 2019;45:166–175. [CrossRef]
[18] Feng J, Chen P, Zhou Q, Dai K, An E, Yuan Y. Numerical simulation of explosive welding using Smoothed Particle Hydrodynamics method. Int J Multiphysics 2017;11:315–326. [CrossRef]
[19] Su Z, Masaki M, Nishida M, Kawase M, Hokamoto K, Inao D. Characteristics of ejecta resulting from hypervelocity impact on Al/Mg explosive welding clad materials. Int J Impact Eng 2024;186:104869. [CrossRef]
[20] Grignon F, Benson D, Vecchio KS, Meyers MA. Explosive welding of aluminum to aluminum: analysis, computations and experiments. Int J Impact Eng 2004;30:1333–1351. [CrossRef]
[21] Chen X, Inao D, Tanaka S, Mori A, Li X, Hokamoto K. Explosive welding of Al alloys and high strength duplex stainless steel by controlling energetic conditions. J Manuf Process 2020;58:1318–1333. [CrossRef]
[22] Saravanan S, Raghukandan K. Microstructure, strength and welding window of aluminum alloy–stainless steel explosive cladding with different interlayers. T Nonferr Metal Soc 2022;32:91–103. [CrossRef]
[23] Elango E, Saravanan S, Raghukandan K. Experimental and numerical studies on aluminum–stainless steel explosive cladding. J Cent South Univ 2020;27:1742–1753. [CrossRef]
[24] Satyanarayan, Tanaka S, Mori A, Hokamoto K. Welding of Sn and Cu plates using controlled underwater shock wave. J Mater Process Technol 2017;245:300–308. [CrossRef]
[25] Somasundaram S, Krishnamurthy R, Kazuyuki H. Effect of process parameters on microstructural and mechanical properties of Ti–SS 304L explosive cladding. J Cent South Univ 2017;24:1245–1251. [CrossRef]
[26] Gülenç B, Kaya Y, Durgutlu A, Gülenç İT, Yıldırım MS, Kahraman N. Production of wire reinforced composite materials through explosive welding. Arch Civil Mech Eng 2016;16:1–8. [CrossRef]
[27] Robin LG, Raghukandan K, Saravanan S. Studies on wire-mesh and silicon carbide particle reinforcements in explosive cladding of Al 1100–Al 5052 sheets. J Manuf Process 2020;56:887–897. [CrossRef]
[28] Kumar P, Ghosh SK, Saravanan S, Barma JD, Meitei RK. Effects of reinforcements in Al 5052 and AZ31B explosively weld composites. Arch Civil Mech Eng 2024;24:1–16. [CrossRef]
[29] Saravanan S, Raghukandan K. Effect of silicon carbide and wire-mesh reinforcements in dissimilar grade aluminium explosive clad composites. Def Technol 2020;16:1160–1166. [CrossRef]
[30] Inao D, Mori A, Tanaka S, Hokamoto K. Explosive welding of thin aluminum plate onto magnesium alloy plate using a gelatin layer as a pressure-transmitting medium. Metals 2020;10:106. [CrossRef]
[31] Chen X, Inao D, Tanaka S, Li X, Bataev IA, Hokamoto K. Comparison of explosive welding of pure titanium/SUS 304 austenitic stainless steel and pure titanium/SUS 821L1 duplex stainless steel. T Nonferr Metal Soc 2021;31:2687–2702. [CrossRef]
[32] Athar MH, Tolaminejad B. Weldability window and the effect of interface morphology on the properties of Al/Cu/Al laminated composites fabricated by explosive welding. Mater Des 2015;86:516–525. [CrossRef]
[33] Saravanan S, Kumararaja K, Raghukandan K. Application of deep learning techniques to predict the mechanical strength of Al–Steel explosive clads. Metals 2023;13:373. [CrossRef]
[34] Kumar CWD, Saravanan S, Raghukandan K. Influence of grooved base plate on microstructure and mechanical strength of aluminum–stainless steel explosive cladding. T Indian I Metals 2019;72:3269–3276. [CrossRef]